Spectral resolved Measurement of the Nitrogen Fluorescence Emissions in Air induced by Electrons

T. Waldenmaier [a,*] J. Blümer [a,b], H. Klages [a]

[a] *Forschungszentrum Karlsruhe, Institut für Kernphysik, P.O.Box 3640, 76021 Karlsruhe, Germany*
[b] *Universität Karlsruhe, Institut für Experimentelle Kernphysik, P.O.Box 6980, 76128 Karlsruhe, Germany*

Abstract

For the calorimetric determination of the primary energy of extensive air showers, measured by fluorescence telescopes, a precise knowledge of the conversion factor (fluorescence yield) between the deposited energy in the atmosphere and the number of emitted fluorescence photons is essential. The fluorescence yield depends on the pressure and the temperature of the air as well as on the water vapor concentration. Within the scope of this work the fluorescence yield for the eight strongest nitrogen emission bands between 300 nm and 400 nm has been measured using electrons from a ^{90}Sr-source with energies between 250 keV and 2000 keV. Measurements have been performed in dry air, pure nitrogen, and a nitrogen-oxygen mixture at pressures ranging from 2 hPa to 990 hPa. Furthermore the influence of water vapor has been studied. A new approach for the parametrization of the fluorescence yield was used to analyze the data, leading to a consistent description of the fluorescence yield with a minimal set of parameters. The resulting absolute accuracies for the single nitrogen bands are in the order of 15 %. In the investigated energy range, the fluorescence yield proved to be independent of the energy of the ionizing electrons.

Key words: air shower, nitrogen, fluorescence yield, quenching, water vapor
PACS: 96.50.sd, 34.80.Gs, 33.50.Dq, 33.50.Hv

1. Introduction

The measurement of air fluorescence is used by many modern experiments (i.e. Pierre Auger Observatory [1], HiRes [2]) to detect extensive air showers (EAS), induced by ultra-high energy cosmic rays. The secondary EAS particles, predominantly electrons and positrons, deposit their energy in the atmosphere by exciting or ionizing the air molecules which afterwards may relax by emitting fluorescence photons. As pointed out by Bunner [3] most of these emissions, in the wavelength range between 300 nm and 400 nm, originate from transitions of neutral or ionized nitrogen molecules. These faint emissions can be measured by fluorescence telescopes, allowing the observation of the longitudinal development of EAS through the atmosphere and a calorimetric determination of the primary cosmic-ray energy. The conversion factor between the deposited energy in the air and the number of emitted fluorescence photons is the so-called fluorescence yield $Y_\lambda(p,T)$ which depends on the air pressure p and temperature T at the place of emission, as well as on the wavelength λ of the emitted photons. If $Y_\lambda(p,T)$ does not depend on the energy of the exciting particles the number of fluorescence photons, observed by a telescope, is directly related to the deposited energy according to

$$\frac{dN_\gamma}{dx} = \frac{dE_{dep}}{dx} \cdot \sum_\lambda Y_\lambda(p,T) \cdot T_{atm}(\lambda,x) \cdot \varepsilon_{det}(\lambda,x) \qquad (1)$$

where dx denotes an interval along the shower axis, $T_{atm}(\lambda,x)$ is the atmospheric transmission factor and $\varepsilon_{det}(\lambda,x)$ corresponds to the detection efficiency of the telescope. The summation goes over all wavelengths λ passing the filter of the telescope, typically ranging from 300 nm to 400 nm. The one dimensional representation above only holds for large distances between the EAS and the telescope where the lateral spread of the EAS can be neglected. Integrating Eq. (1) over x results in the total electromagnetic energy of the EAS and thus is the most direct measure of the primary cosmic ray energy. The precision of this method is, however, limited by the present

* Current address of corresponding author:
Bartol Research Institute, DPA, University of Delaware,
Newark, DE 19716 , U.S.A.
Email address: tilo@bartol.udel.edu (Tilo Waldenmaier)

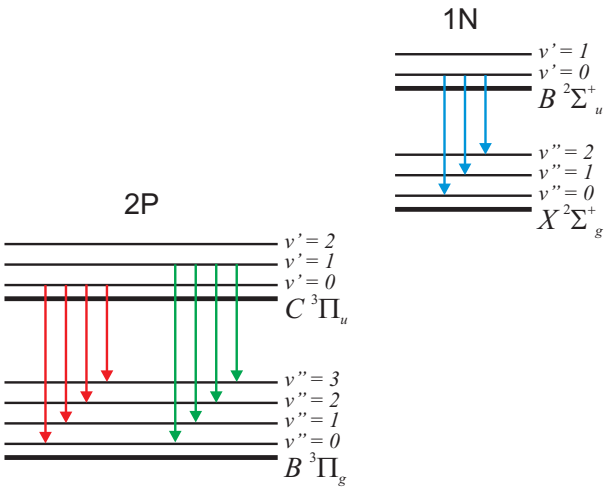

Fig. 1. Scheme of the energy states of the 2P and 1N electronic-vibrational band systems of N_2 and N_2^+. The corresponding spectral bands in Fig. 2 are drawn in the same colors.

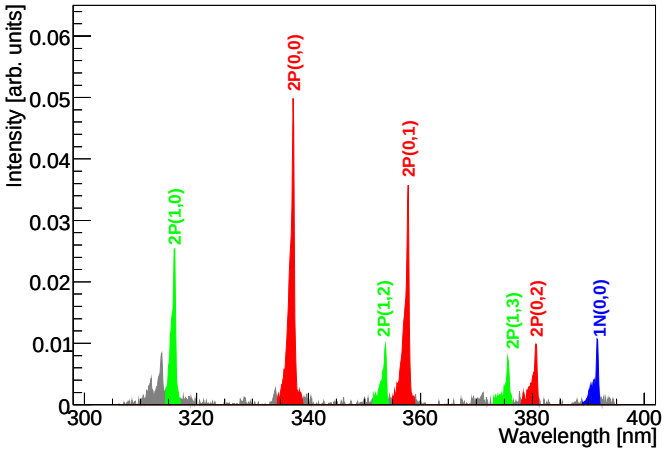

Fig. 2. Nitrogen fluorescence spectrum between 300 nm and 400 nm in dry air at 1013 hPa measured by Ulrich et al. [10].

uncertainties of the fluorescence yield of about 15 % to 30 % and the lack of knowledge about its energy dependence. In recent years this gave rise to a number of new laboratory experiments, i.e. Kakimoto et al. [4], Nagano et al. [5,6], AIRFLY [7], FLASH [8] or **AirLight**, aiming at a precise measurement of the fluorescence yield over a wide energy, pressure and temperature range.

This paper reports on the data analysis and the results of the **AirLight** experiment at Forschungszentrum Karlsruhe in Germany. Section 2 describes the process of nitrogen fluorescence in air and introduces a new approach to model the fluorescence yield in a consistent way and with a minimal set of parameters. The experimental setup is addressed in Section 3 and finally the data analysis and the results are discussed in Section 4 and 5. This paper is extracted from the Ph.D. thesis [9] of the corresponding author which can be referred for more details. Some changes have been applied to correct minor errors and to improve the readability.

2. Nitrogen Fluorescence in Air

Nearly all the air fluorescence emissions in the wavelength range between 300 nm and 400 nm originate from neutral or ionized nitrogen molecules [3,11]. The fluorescence spectrum of molecular nitrogen is a band spectrum. In contrast to atomic line spectra, molecular spectra consist of a variety of broad bands. This band structure is caused by the vibrational and rotational movements of the molecular nuclei which modify the energy states of the electrons. For diatomic, homo-nuclear molecules the energy of a molecular state can be expressed as the sum of three contributions

$$E = E_{el} + E_{vib} + E_{rot} \quad , \tag{2}$$

where E_{el} is the potential electron energy of a static molecule and E_{vib} and E_{rot} are additional contributions due to vibrations and rotations of the molecular nuclei. This approach is known as the Born-Oppenheimer approximation [12,13]. The energy scales of the three contributions are very different and approximately behave like

$$E_{el} : E_{vib} : E_{rot} = 1 : \sqrt{\frac{m}{M}} : \frac{m}{M} \quad , \tag{3}$$

where m is the electron mass and M denotes the mass of the molecular nuclei [12]. This causes an electronic molecular state to split into several vibrational levels and every vibrational level again has a rotational substructure, as is illustrated in Fig. 1. Very often the rotational substructure is not resolved, which leads to the observation of vibrational bands with a sharp edge at one side and a shading to the other side, as can be seen in Fig. 2. Since the rotational substructure plays no role for the application on EAS measurements it will be disregarded in the following.

An "electronic band system" is established by all electronic-vibrational transitions having the same initial and final electronic states. The nitrogen fluorescence spectrum between 300 nm and 400 nm nearly entirely consists of transitions of the "second positive" (2P) band system [1] of N_2 and the "first negative" (1N) band system of N_2^+ [3,11]. The spectroscopic notation for these transitions is given by

– 2P-System: $C^3\Pi_u(v') \rightarrow B^3\Pi_g(v'')$

– 1N-System: $B^2\Sigma_u^+(v') \rightarrow X^2\Sigma_g^+(v'')$

where the quantum numbers v' and v'' of the initial and final vibrational levels are written within the parentheses behind the symbols for the electron configuration of the corresponding molecular state. Accordingly these transi-

[1] The notation "first negative" and "second positive" system indicates the place of appearance of the corresponding light emissions in gas discharge tubes. "Negative" systems appear closer to the cathode whereas "positive" systems are attracted by the anode.

tions are denoted as $2P(v', v'')$ in case of the 2P-System and $1N(v', v'')$ for the 1N-System. In the following the symbols v' and v'' always denote initial and final electronic-vibrational states of a certain electronic band system. Any numerical values of v' or v'' indicate the vibrational level of the corresponding electronic state. Pure vibrational transitions are not a subject of the following discussions.

2.1. *De-Excitation*

Assuming a number of excited nitrogen molecules in a certain electronic-vibrational state v' and neglecting any kind of cascading into this state, the deactivation rate can be calculated according to the general decay law

$$\frac{dN_{v'}}{dt} = -\underbrace{\Big(\lambda_{rest} + \sum_{v''} A_{v',v''}\Big)}_{\lambda_{v'}} \cdot N_{v'}(t) \quad , \tag{4}$$

where $N_{v'}(t)$ denotes the number of molecules in the state v' at a certain time t. The total decay constant $\lambda_{v'}$, which equals the reciprocal mean lifetime $\tau_{v'}$ of the state v', is the sum of the decay constants of all potential decay channels. The quantities $A_{v',v''}$ denote the decay constants or transition probabilities for all radiative transitions $v' \rightarrow v''$ within the underlying band system and are also known as Einstein coefficients. A detailed list of Einstein coefficients of many nitrogen and oxygen band systems can be found in the comprehensive work of Gilmore et al. [14]. In addition, there might be any kind of other radiating or non-radiating transitions which are summarized in the common decay constant λ_{rest}. From Eq. (4) two fundamental properties can be immediately derived:

(i) The measurable mean lifetime $\tau_{v'}$ of an electronic-vibrational state v' is the same for all transitions $v' \rightarrow v''$ originating from this state.

(ii) The intensity ratios between spontaneous transitions of the same electronic-vibrational state v' are constant and correspond to the ratios of their Einstein coefficients $A_{v',v''}$.

The latter property causes the 2P and 1N band systems of the nitrogen spectrum to be assembled from several sub-spectra for each vibrational level v', as is illustrated in Fig. 2. In the wavelength range between 300 nm and 400 nm the most intensive nitrogen transitions of the 2P system originate from the vibrational levels $v' = 0, 1$, whereas the 1N system has just one notable transition 1N(0,0) at 391.4 nm. For each of these sub-spectra the intensity ratios between their vibrational bands are constant, but the absolute normalization of each sub-spectrum in general changes differently with pressure and temperature, as will be explained in the following.

2.2. *Radiationless Deactivations: Quenching*

An excited electronic-vibrational state v' can also become de-activated by radiationless processes such as rotational, vibrational or translational energy transfer during collisions with other molecules [13]. These so-called quenching processes strongly depend on the number density ($\rightarrow$ Pressure) and the velocity ($\rightarrow$ Temperature) of the colliding molecules.

Assume an excited nitrogen molecule in the state v' hitting a gas target where the target molecules are at rest. Under such conditions a collisional deactivation constant $\lambda_{c,x}^{v'}$ can be defined according to

$$\lambda_{c,x}^{v'} = n_x \cdot \sigma_{N_2,x}^{v'}(v_{rel}) \cdot v_{rel} \quad , \tag{5}$$

where n_x is the number density of the target molecules of type x and $\sigma_{N_2,x}^{v'}(v_{rel})$ denotes the total collisional cross-section for the deactivation of a nitrogen molecule in the state v' which was injected with a relative velocity v_{rel} with respect to the target molecules. In reality, the projectile is part of the target gas and the Maxwell-Boltzmann distribution applies for the velocities of the target and projectile molecules. Therefore Eq. (5) has to be averaged over all relative velocities v_{rel} between the colliding molecules [3,9]. The collisional cross-sections $\sigma_{N_2,x}^{v'}(v_{rel})$ in general depend on the relative velocities v_{rel} and thus on the temperature of the gas. At present, no temperature dependence has been reported and therefore $\sigma_{N_2,x}^{v'}$ in the following is assumed to be constant. In this approximation, averaging over the molecular velocities in Eq. (5) leads to the expression

$$\lambda_{c,x}^{v'} = n_x \cdot \underbrace{\sigma_{N_2,x}^{v'} \cdot \langle v_{N_2} \rangle \cdot \sqrt{\frac{m_{N_2} + m_x}{m_x}}}_{=:\, Q_x^{v'}(T)} \quad , \tag{6}$$

where $\langle v_{N_2} \rangle = \sqrt{8kT/\pi m_{N_2}}$ is the mean velocity of the nitrogen molecules at temperature T according to the Maxwell-Boltzmann distribution and m_x is the mass of the target molecules of type x. It is convenient to introduce a quenching rate constant $Q_x^{v'}(T)$ for each gas constituent x. Since $Q_x^{v'}(T)$ depends on $\langle v_{N_2} \rangle$ it is not a real constant, but it is proportional to $\sqrt{T}$ if no additional temperature dependence from the collisional cross-sections $\sigma_{N_2,x}^{v'}$ has to be taken into account. All the quenching rate constants in this paper are quoted for a temperature of 293 K ($\sim 20°C$). Quenching rate constants for other temperatures can be computed according to

$$Q_x^{v'}(T) = \sqrt{\frac{T}{293\ K}} \cdot Q_x^{v'}(293\ K) \ . \tag{7}$$

If the gas is a mixture of different constituents x, the total collisional deactivation constant $\lambda_c^{v'}$ is the sum of the deactivation constants of all gas constituents:

$$\lambda_c^{v'} = \sum_x \lambda_{c,x}^{v'} = \sum_x n_x \cdot Q_x^{v'}(T)$$
$$= \frac{p}{kT} \sum_x f_x \cdot Q_x^{v'}(T) =: C_{v'} \frac{p}{\sqrt{T}} \quad . \tag{8}$$

The last expression is proportional to $p/\sqrt{T}$ by a factor $C_{v'}$ and was obtained by substituting the number densities n_x through the partial pressures $p_x = n_x kT$, as follows from the ideal gas law. In a second step the partial pressures p_x have been expressed as $p_x = f_x \cdot p$, where f_x denotes the relative abundance of the different gas constituents, e.g. for dry air $f_{N_2} = 0.78$, $f_{O_2} = 0.21$ and $f_{Ar} = 0.01$.

With this definition for the collisional deactivation constant $\lambda_c^{v'}(p,T)$ the total decay constant or reciprocal lifetime $1/\tau_{v'}$ of an electronic vibrational state v' can be expressed as

$$\frac{1}{\tau_{v'}(p,T)} = \lambda_c^{v'}(p,T) + \underbrace{\lambda_{rest}^{v'} + \sum_{v''} A_{v',v''}}_{=:\ 1/\tau_0^{v'}} \quad , \tag{9}$$

where $\lambda_{rest}^{v'}$ incorporates the decay constants for all remaining deactivations or transitions with constant transition probabilities. At zero pressure $\lambda_c^{v'}(p,T)$ vanishes and the total lifetime $\tau_{v'}(p,T)|_{p=0}$ becomes equal to the intrinsic lifetime $\tau_0^{v'}$, which is the reciprocal sum of all constant transition probabilities.

Instead of the quenching rate constants $Q_x^{v'}(T)$, it is sometimes more convenient to introduce a reference pressure $p'_{v'}(T)$ for a given gas mixture. The reference pressure $p'_{v'}(T)$ is defined as the pressure where the collisional deactivation constant $\lambda_c^{v'}(p,T)$ equals the reciprocal intrinsic lifetime $1/\tau_0^{v'}$. With this definition Eq. (9) transforms to the simple form

$$\frac{1}{\tau_{v'}(p,T)} = \frac{1}{\tau_0^{v'}} \cdot \left(1 + \frac{p}{p'_{v'}(T)}\right) \ , \ p'_{v'}(T) = \frac{\sqrt{T}}{C_{v'}\tau_0^{v'}} \ , \tag{10}$$

which immediately reveals the linear pressure dependence of the reciprocal lifetime $1/\tau_{v'}(p,T)$ for a constant temperature.

2.3. *Excitation: Intrinsic Fluorescence Yield*

The excitation of the relevant molecular nitrogen states in EAS generally occurs via many different processes. The initial electronic state $B^2\Sigma_u^+$ of the 1N system is usually activated through the direct ionization of neutral nitrogen molecules by high energy electrons

$$\mathrm{e} + \mathrm{N}_2\left(X^1\Sigma_g^+\right) \longrightarrow \mathrm{N}_2^{+*}\left(B^2\Sigma_u^+\right) + \mathrm{e} + \mathrm{e} \quad , \tag{11}$$

whereas the excitation of the $C^3\Pi_u$ state of the 2P system mainly occurs via low energy secondary processes such as the recombination of ionized nitrogen molecules

$$\mathrm{e} + \mathrm{N}_2^+\left(X^2\Sigma_g^+\right) \longrightarrow \mathrm{N}_2{}^*\left(C^3\Pi_u\right) \quad , \tag{12}$$

or the direct excitation from the ground state

$$\mathrm{e}(\uparrow) + \mathrm{N}_2\left(X^1\Sigma_g^+\right) \longrightarrow \mathrm{N}_2{}^*\left(C^3\Pi_u\right) + \mathrm{e}(\downarrow) \quad . \tag{13}$$

The latter process, to the first order, is forbidden, since it requires a change in the spin quantum number of the molecular state. Nevertheless, this excitation becomes possible for low energy electrons via electron exchange if spin-orbit-coupling is taken into account [3,13].

In general, an electron releases its energy in a series of different processes and only a small fraction of the energy, which was deposited in a certain volume, is finally converted into fluorescence photons. Thus if $\aleph_{v'}(E)$ is the number of nitrogen molecules per deposited energy which have been excited into the state v', the fluorescence yield $Y_{v',v''}(E,p,T)$ for the radiative transition $v' \to v''$, in units of photons per deposited energy, can be expressed as

$$Y_{v',v''}(E,p,T) = \aleph_{v'}(E) \cdot A_{v',v''} \cdot \tau_{v'}(p,T)$$
$$= \underbrace{\aleph_{v'}(E) \cdot A_{v',v''} \cdot \tau_0^{v'}}_{=:\ Y^0_{v',v''}(E)} \cdot \frac{\tau_{v'}(p,T)}{\tau_0^{v'}} \quad . \tag{14}$$

The term $A_{v',v''} \cdot \tau_0^{v'}$ in the final expression determines the probability for an excited state v' to relax via the transition $v' \to v''$ if collisional quenching effects are neglected. Therefore, the intrinsic fluorescence yield $Y^0_{v',v''}(E)$ is defined as the number of emitted fluorescence photons per deposited energy in the absence of collisional quenching. The collisional quenching is finally taken into account by the separate factor $\tau_{v'}(p,T)/\tau_0^{v'}$ which determines the fraction of excited states v' which are not going to be deactivated by collisional processes. This approach naturally separates between excitation and de-excitation processes. Potential energy dependencies of the effective excitation process only affect the intrinsic fluorescence yield $Y^0_{v',v''}(E)$, whereas pressure and temperature only act on the quenching and thus on the lifetime $\tau_{v'}(p,T)$.

As pointed out in Section 2.1, the intensity ratios between transitions emerging from the same electronic-vibrational state v' are always constant. In order to apply this relation to Eq. (14), a main-transition $v' \to k$ needs to be specified for each initial vibrational state v'. A main-transition is defined as the most intensive transition of the corresponding vibrational sub-system, but in principle the choice is completely arbitrary. In this work the main-transitions for the investigated band systems have been chosen to be 2P(0,0), 2P(1,0) and 1N(0,0). Now the intensity ratio $R_{v',v''}$ of a transition $v' \to v''$ can be quoted with respect to the main-transition as the ratio of the corresponding Einstein-coefficients:

$$R_{v',v''} = \frac{A_{v',v''}}{A_{v',k}} \quad , \tag{15}$$

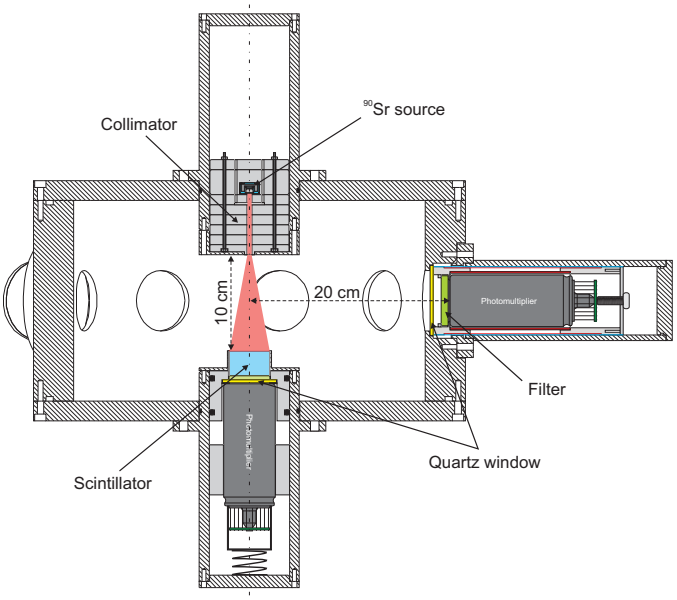

Fig. 3. Sketch of the AirLight chamber. After exiting the collimator the electrons traverse 10 cm of gas before they are stopped in the scintillator. Seven PMTs, equipped with different filters, measure the fluorescence emissions perpendicularly to the electron beam.

All main-transitions have $R_{v',k} \equiv 1$. With these definitions Eq. (14) transforms to the final expression

$$Y_{v',v''}(E,p,T) = Y^0_{v',k}(E) \cdot R_{v',v''} \cdot \frac{\tau_{v'}(p,T)}{\tau_0^{v'}} \quad , \qquad (16)$$

where $Y^0_{v',k}(E)$ denotes the intrinsic fluorescence yield of the main-transition. All quantities in this equation now have a clear physical meaning and are able to be measured experimentally. Furthermore, all transitions emerging from the same initial state v' are treated consistently with a minimal set of parameters.

In previous papers the fluorescence yield is often defined as the number of emitted fluorescence photons per meter track length of the ionizing particle. This definition has several disadvantages as will be explained in the following. First of all it requires all secondary electrons to be tracked as well in order to obtain correct results. Since the field of view of all laboratory experiments is limited to a relatively small region around the electron beam, secondary electrons can easily escape and thus do not contribute to the fluorescence emissions in this volume. It is even possible that electrons are scattered back from the chamber walls into the field of view and induce additional fluorescence photons. All these effects are very difficult to treat if the fluorescence yield is defined as photons per meter. Instead it is relatively simple to retrieve the deposited energy in a certain volume by Monte Carlo simulations (see Section 4.3.1) and to determine the number of fluorescence photons per deposited energy, which accounts for all effects mentioned above. Another drawback of the definition in photons per meter is that the fluorescence yield depends on the underlying energy loss model as well as on the energy and the pressure, which makes it rather difficult to compare values of different authors. All these problems diminish if the fluorescence yield is defined as photons per deposited energy, which seems also to be more natural, since the deposited energy is the maximum energy which may dissipate into fluorescence photons. This definition is much more convenient, particularly for EAS measurements, since it allows the number of observed photons to be directly converted into an energy deposit profile of the EAS by means of Eq. 1. Therefore, the fluorescence yield in this paper is always defined as photons per deposited energy. The "old" definition in terms of photons per meter can be obtained by multiplying the fluorescence yield with an appropriate energy loss function $\frac{dE}{dx}$.

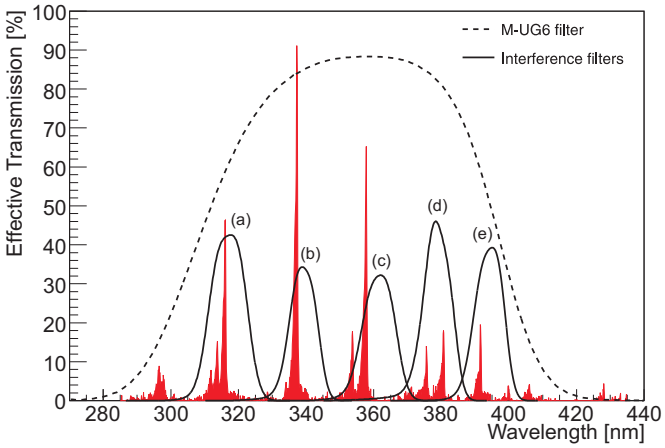

Fig. 4. Effective transmission curves of the interference filters (solid lines) and the broad band M-UG6 filter (dashed line) overlaid with a nitrogen fluorescence spectrum measured by Ulrich et al. [10].

3. The AirLight Experiment

The AirLight experiment [9] at Forschungszentrum Karlsruhe was designed to measure all the different quantities in Eq. (16). The experimental setup is similar to the experiments done by Kakimoto and Nagano et al. [4,5,6]. As is shown in Fig. 3 it consists of a cylindrical aluminum chamber in which electrons are injected along the chamber axis. The electrons are emitted from a ^{90}Sr-source situated at the top of the chamber. The source has an activity of 37 MBq with an end point energy of 2.3 MeV. The electrons are collimated by massive lead rings with an inner diameter of 5 mm, before they enter the inner volume of the chamber. After traversing 10 cm of gas (dry air, pure nitrogen, or a nitrogen-oxygen mixture) they are finally stopped in a plastic scintillator of 2.5 cm height and 4 cm diameter [9]. The plastic scintillator measures the energy of the electrons with an energy resolution of about 10 % at 1 MeV. The electron rate at the scintillator varies between 10 kHz and 20 kHz, depending on the pressure in the chamber which can be adjusted between 2 hPa and 1000 hPa.

Due to the relatively low electron rate the intensity of the electron-induced fluorescence light is not sufficient to

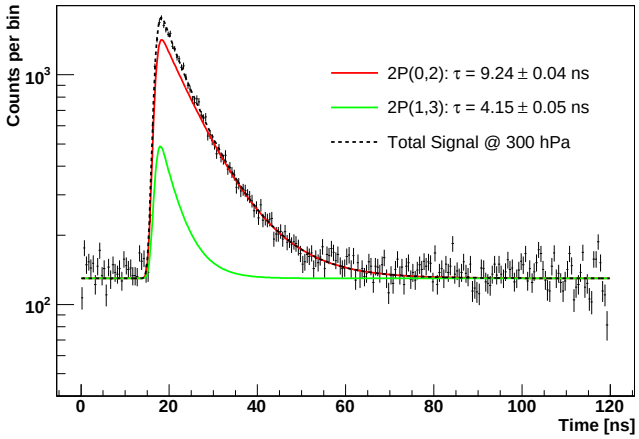

Fig. 5. Exponential time distribution between the electron signals in the scintillator and the photon signals in channel 3. The equally distributed offset is due to accidental coincidences (thermal noise) in the PMT. The total fluorescence signal in this channel is a superposition of the 2P(0,2) and the 2P(1,3) transitions.

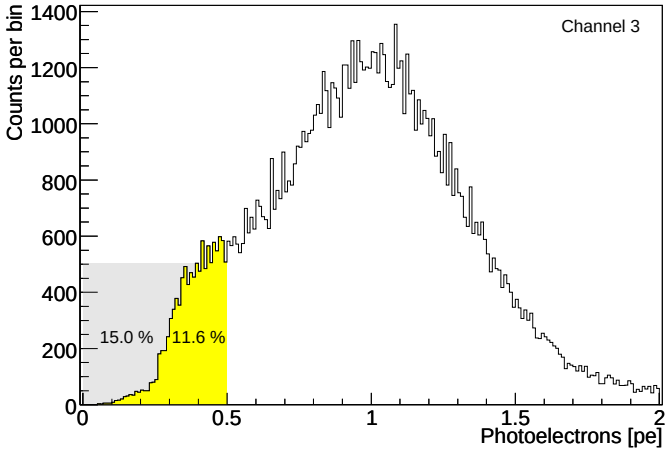

Fig. 6. Single photoelectron distribution of channel 3. Only signals between 0.5 pe and 2 pe are considered in the data analysis. Roughly 11.6 % of the signals are between the discriminator threshold and 0.5 pe (yellow region). The gray region is a crude estimate of 15 % for the signals below the discriminator threshold.

allow the use of a spectrometer or monochromator to make a spectral resolved measurement. Therefore, seven 2" Photonis photomultipliers [2] (PMT) equipped with different filters are mounted perpendicularly, at a distance of 20 cm, to the chamber axis to measure the fluorescence photons in several wavelength ranges. The active area of each of the photocathodes is defined by a 4 cm aperture. As shown in Fig. 4, the set of filters consists of one broad band M-UG6 absorption filter ranging from 300 nm to 410 nm, identical to those used in the fluorescence telescopes of the Pierre Auger Observatory [1], and six narrow band interference filters matched to the most prominent nitrogen bands. Since interference filters are known to change their transmission characteristics with the incident angle of the light, the effective transmission functions plotted in Fig. 4 were obtained by averaging over the angle distribution of the fluorescence photons [15,9] which was determined by means of Monte Carlo simulations [9]. The pressure dependence of the angular distribution, due to the multiple scattering of the electrons, turned out to be negligible.

The experiment measures coincidences between individual electron signals in the scintillator and single photon signals in any of the PMTs. The coincidence condition is fulfilled if a photon signal appears within an interval of 120 ns after an electron signal was detected. The distribution of time differences (see Fig. 5) between electron and photon signals, as well as the single photoelectron distributions (see Fig. 6), are sampled for each filter channel by a CAEN V488 TDC [3] and a Lecroy 1182 ADC [4]. One ADC channel is sampling the energy distributions of the electrons. After every tenth coincidence, the coincidence condition is disabled for the next electron to measure also the unbiased (free) electron energy spectrum. Finally the absolute numbers of free and coincident photon and electron triggers are counted by a CAEN V260 scaler module with a guaranteed input frequency of 100 MHz. The typical free rates of the photon detectors at 20 °C ranged from 400 Hz to 600 Hz.

By means of the TDC time spectra, fluorescence signals can be clearly discriminated from accidental coincidences. As is shown in Fig. 5 the time distribution of the fluorescence photons follows an exponential decay law as is expected from Eq. (4). Contrary to this, accidental coincidences show a flat distribution, since the timing of the electron and photon signals is completely uncorrelated. The time resolution σ_t of each filter channel is of the order of 0.7 ns. Therefore, the time distribution of the fluorescence signals can be described by a convolution of an exponential- and a Gaussian function with $\sigma = \sigma_t$ which is given by the expression

$$\frac{dN}{dt} = \frac{1}{2}\frac{N}{\tau} \cdot e^{-\frac{t-t_0}{\tau}} \cdot e^{\frac{\sigma_t^2}{2\tau^2}} \cdot \mathrm{erfc}\left(\frac{t_0 - t + \frac{\sigma_t^2}{\tau}}{\sqrt{2}\sigma_t}\right) \quad . \qquad (17)$$

The time integral of this function corresponds to the total number of fluorescence photons N, whereas τ denotes the lifetime of the emitting nitrogen state. As can be seen in Fig. 5 the time origin t_0 is in the order of 16 ns and is roughly the same in all filter channels. In general there are several nitrogen bands with different lifetimes τ overlapping in one filter channel. Therefore, the measured time distribution results from a superposition of several distributions given by Eq. (17) with different lifetimes and intensities but with the same values for the time origin and time resolution of the relevant filter channel.

The number of detected photons N_{det}^i in a filter channel i is linked to the real number of emitted photons N through the relation

[2] Photonis PMT types: XP2262, XP2268
[3] TDC: Time to Digital Converter
[4] ADC: Analog to Digital Converter

$$N^i_{det} = N \cdot \underbrace{\varepsilon^i_{cut} \cdot \varepsilon^i_{col} \cdot f_i}_{f^i_{cal}} \cdot \varepsilon_\Omega \underbrace{\int_\lambda \varepsilon^0_{QE}(\lambda) \cdot T(\lambda) \cdot \frac{d\hat{N}}{d\lambda}\, d\lambda}_{\varepsilon^i_s} \quad (18)$$

The integral in this expression corresponds to the spectral efficiency ε^i_s, which contains the nominal quantum efficiency function $\varepsilon^0_{QE}(\lambda)$ of the PMT, as quoted by the manufacturer, the effective transmission function $T(\lambda)$ of the filter and the normalized spectral distribution $\frac{d\hat{N}}{d\lambda}$ of the emitted photons. If the spectral distribution is known, the integral ε^i_s can be easily computed, since the unknown normalization factor f_i of the individual quantum efficiency function $\varepsilon^i_{QE}(\lambda) = f_i \cdot \varepsilon^0_{QE}(\lambda)$ has been moved out of the integral. The PMT acceptance is given by the geometrical factor ε_Ω which is the same for all filter channels, since the whole setup is completely symmetric against the chamber axis. For fluorescence measurements ε_Ω has been determined by means of Monte Carlo simulations to a value of (0.2586 ± 0.0003) % which doesn't depend on the pressure. The collection efficiency ε^i_{col} of the PMTs is assumed to be constant over the relatively small filter range. Finally we must account for the cut efficiency ε^i_{cut}, since only photon signals between 0.5 pe and 2.0 pe [5] are used in the data analysis as illustrated in Fig. 6. The normalization factor f_i, the collection efficiency ε^i_{col} and the cut efficiency are the only unknown quantities in Eq. (18). For convenience they have been merged into the final calibration constant f^i_{cal}.

3.1. *Absolute Calibration*

In principle the calibration constants f^i_{cal} can be individually determined by a calibration measurement where a well calibrated light source is placed in the center of the chamber. In the present work it was not possible to perform such an end-to-end calibration since an appropriate light source was not yet available. Nevertheless a relative calibration has been performed where an uncalibrated but stable and axial symmetric light source with a well known spectrum was used instead. Furthermore the filters in front of the PMTs have been removed, resulting in $T(\lambda) \equiv 1$ for each channel. This way all PMTs are illuminated with an equal but unknown amount of photons and the acceptance ε_Ω is the same for all channels due to symmetry reasons. By means of Eq. (18) the calibration constants f^i_{cal} have been relatively determined according to

$$\frac{N^i_{det}}{N^3_{det}} = \frac{f^i_{cal} \cdot \varepsilon^i_s}{f^3_{cal} \cdot \varepsilon^3_s} \quad \Longleftrightarrow \quad f^i_{cal} = \frac{\varepsilon^3_s}{\varepsilon^i_s} \cdot \frac{N^i_{det}}{N^3_{det}} \cdot f^3_{cal} \quad , \qquad (19)$$

where channel 3 was chosen for technical reasons to be the reference channel. In case of equal PMT types the spectral efficiencies ε^i_s cancel and the calibration constant is just the fraction of the detected photons with respect to the reference channel times the reference constant. In order to evaluate absolute values for the calibration constants, the reference constant f^3_{cal} was estimated under the following conditions:

The shape of the single photoelectron distribution of the reference channel, shown in Fig. 6, as well as the discriminator threshold are assumed to be stable over the whole period of measurements. Stable photoelectron distributions are also required for all the other channels. Furthermore, the photoelectron distributions of accidental coincidences, which are mainly caused by thermal noise of the PMTs, must be roughly the same as for real photon signals. These requirements have been proven to be satisfactorily fulfilled over the whole data-taking period [9].

The area between 0.5 pe and 2.0 pe in the single photoelectron distribution shown in Fig. 6 corresponds to 100 % of the detected photons which have been considered in the data-analysis. Signals above 2.0 pe are mainly due to noise or background and can be neglected. However, roughly 12 % of the signals are situated between the discriminator threshold and the quality cut at 0.5 pe (yellow region) and have to be taken into account. The number of signals between the pedestal at 0 pe and the discriminator threshold (gray region) is unknown but has been conservatively estimated to be less than 15 % of the detected signals. Therefore, half of this value (7.5 %) is added to the number of detected signals and the other 7.5 % are taken as the systematic uncertainty of this estimation. Thus, if N_{cut} denotes the number of signals ranging from 0.5 pe to 2.0 pe, the real number of signals N_{real} can be evaluated by the expression

$$N_{real} = (100\ \% + 12\ \% + 7.5\ \% \pm 7.5\ \%) \cdot N_{cut} \quad , \qquad (20)$$

which finally results in an estimation for the cut efficiency of channel 3:

$$\varepsilon^3_{cut} = \frac{N_{cut}}{N_{real}} = \frac{1}{(1.195 \pm 0.075)} = 0.837 \pm 0.053 \quad . \qquad (21)$$

The PMT quantum efficiency function $\varepsilon^3_{QE}(\lambda)$ of channel 3, with a maximum value of 26.6 % at 420 nm, is assumed to be known with an uncertainty of 5 %, which implies a normalization factor $f_3 = 1.00 \pm 0.05$. For the collection efficiency ε^3_{col} a value of 0.880 ± 0.088 has been assumed. Using these values the absolute calibration factor f^3_{cal} of the reference channel 3 can be estimated according to

$$f^3_{cal} = \varepsilon^3_{cut} \cdot \varepsilon^3_{col} \cdot f_3 = 0.737 \pm 0.095 \quad , \qquad (22)$$

with a systematic uncertainty of about 13 %. By means of Eq. (19) the calibration constants of the other channels can be derived relative to f^3_{cal}. Relative calibration measurements have been performed once a month over the whole data-taking period and turned out to be extremely stable [9]. The resulting detection efficiencies $\varepsilon_{det} = f_{cal} \cdot \varepsilon_\Omega \cdot \varepsilon_s$

[5] [pe]: photoelectrons

Table 1
Overview of the different filter channels and the corresponding nitrogen bands. The detection efficiencies are determined according to $\varepsilon_{det} = f_{cal} \cdot \varepsilon_\Omega \cdot \varepsilon_s$, using a common acceptance value of $\varepsilon_\Omega = 0.2586$ %. The last column of the table indicates the relative systematic errors $\Delta\varepsilon_{det}$.

Channel	Filter	f_{cal}	Band	λ [nm]	ε_s	ε_{det} [‰]	$\Delta\varepsilon_{det}$ [%]
0	M-UG6	0.832 ± 0.109	2P(1,0)	315.9	0.077 ± 0.006	0.166 ± 0.025	14.93
			2P(0,0)	337.1	0.158 ± 0.008	0.340 ± 0.048	14.09
			2P(1,2)	353.7	0.192 ± 0.009	0.413 ± 0.057	13.86
			2P(0,1)	357.7	0.196 ± 0.009	0.422 ± 0.058	13.84
			2P(1,3)	375.5	0.200 ± 0.008	0.430 ± 0.059	13.76
			2P(0,2)	380.5	0.194 ± 0.008	0.418 ± 0.057	13.74
			1N(0,0)	391.4	0.152 ± 0.006	0.327 ± 0.045	13.68
			2P(1,4)	399.8	0.085 ± 0.003	0.183 ± 0.025	13.68
1	(a)	0.714 ± 0.094	2P(1,0)	315.9	0.094 ± 0.004	0.173 ± 0.024	13.99
2	(c)	0.825 ± 0.108	2P(1,2)	353.7	0.014 ± 0.001	0.029 ± 0.004	15.39
			2P(0,1)	357.7	0.053 ± 0.003	0.112 ± 0.016	14.03
3*	(d)	0.737 ± 0.095	2P(1,3)	375.5	0.078 ± 0.004	0.148 ± 0.020	13.61
			2P(0,2)	380.5	0.106 ± 0.005	0.202 ± 0.027	13.53
4	(b)	0.854 ± 0.114	2P(0,0)	337.1	0.060 ± 0.003	0.133 ± 0.019	14.38
5	(e)	0.788 ± 0.104	1N(0,0)	391.4	0.081 ± 0.004	0.165 ± 0.023	13.84
			2P(1,4)	399.8	0.042 ± 0.002	0.085 ± 0.012	14.08

* Reference channel.

for each nitrogen band in the different filter channels, have been calculated assuming a line spectrum and are listed in Table 1. The corresponding systematic errors are the major source of uncertainty for the absolute determination of the fluorescence yield. Further details about the experiment and the calibration procedures can be found in [9].

4. Measurements & Data Analysis

The data presented in this work were taken from August to November 2005 consisting of about 50 runs in pure nitrogen ($f_{N_2} = 1.00$), dry artificial air ($f_{N_2} = 0.78$, $f_{O_2} = 0.21$, $f_{Ar} = 0.01$) and a nitrogen-oxygen mixture ($f_{N_2} = 0.90$, $f_{O_2} = 0.10$) to reveal the quenching effects of the different air constituents. In addition several runs with pure nitrogen plus a variable amount of water vapor have been performed. The measurements were done at pressures ranging from 2 hPa to 990 hPa at room temperatures between 15 °C and 23 °C, varying with the outside weather conditions. In order to accumulate sufficient statistics, a single run lasted between 12 and 30 hours, depending on the gas mixture and the pressure. Before each run the chamber was flushed and filled with fresh gas to avoid aging and contamination effects. Extensive calibration measurements [9] were carried out before each series of runs with a certain gas.

4.1. *Global Minimization Function*

Challenging for the data analysis are filter channels containing more than one nitrogen band, as is illustrated in Fig. 4. The only channel with a nearly pure contribution of a single nitrogen transition is channel 4 which is measuring the prominent 2P(0,0) band at 337.1 nm. Therefore, the main task for the data analysis is the separation of the different contributions in the individual filter channels. This can be achieved to some extend by a global analysis of the complete set of measurements, making use of the physical relations between the different nitrogen bands, as discussed in Section 2. Technically this was done by a constrained χ^2-minimization of all datasets, where a dataset consists of the synchronous data of all filter channels of a run with a certain gas at a certain pressure. The most universal constraints directly follow from the general decay law (4) and require identical lifetimes $\tau_{v'}(p,T)$ and intrinsic yields $Y^0_{v'}$ for nitrogen bands emerging from the same initial state v' in all filter channels of a dataset. Furthermore, the intensity ratios $R_{v',v''}$ of transitions from the same initial state v' must have the same values in all datasets and therefore

link different runs with each other. These constraints are always valid since they do not depend on any assumption about the excitation or de-excitation mechanism. To further improve the results additional, model dependent, constraints may be applied such as the linear pressure dependence of the reciprocal lifetimes as follows from Eq. (10). This global approach directly results in a consistent description of the fluorescence yield with a minimal set of parameters. Accordingly, the global minimization function was constructed as a sum over all datasets d, filter channels c and time bins b of the corresponding time distributions:

$$\chi^2 = \sum_d \sum_{c=1}^{5} \sum_b \left[\frac{y_{dcb} - (O_{dc} + B_{dcb} + S_{dcb})}{\sigma_{y_{dcb}}} \right]^2 \quad . \qquad (23)$$

In this expression, y_{dcb} denotes the bin content with statistical error $\sigma_{y_{dcb}} = \sqrt{y_{dcb}}$ and O_{dc} corresponds to the constant noise offset per bin of filter channel c in the dataset d. The noise offset O_{dc} was individually determined for each time distribution (see Fig. 5) by averaging over the bins between 2 ns and 12 ns in front of the rising edge of the fluorescence signal. The electron correlated background B_{dcb} was determined and parametrized by means of background measurements with a completely evacuated chamber. Its origin was not fully understood, however it is only relevant for low pressure measurements [9]. Finally the total fluorescence signal S_{dcb} in each bin b is a sum over all nitrogen transitions contributing to this channel

$$S_{dcb} = \varepsilon_{DAQ}^{dc} \cdot \sum_{v',v''} \varepsilon_{det}^{cv'v''} \cdot F_b(R_{v',v''} \cdot N_{dv'},\ \tau_{dv'}) \quad , \qquad (24)$$

where the summation is done over all initial electronic-vibrational states v' as well as over the final states v''. Note that in the case of contributions from different electronic band systems the summation over v' includes the summation over the electronic band systems as well! The function $F_b(R_{v',v''} \cdot N_{dv'},\ \tau_{dv'})$ is the integral of Eq. (17) over the width of bin b and depends on the lifetime $\tau_{dv'}$ of the initial state v' and on the total number of emitted photons by the transition $v' \rightarrow v''$ which are related to the total amount of photons $N_{dv'}$ of the main-transition by $R_{v',v''} \cdot N_{dv'}$. In addition, even if not explicitly quoted in Eq. (24), F_b depends on the time origins t_0 and time resolutions σ_t of each channel which are kept at the same values in all datasets during the minimization procedure. In order to retrieve the number of sampled signals S_{dcb}, each integral function F_b must be multiplied by the detection efficiency $\varepsilon_{det}^{cv'v''}$ of the corresponding transition and the data acquisition efficiency ε_{DAQ}^{dc} (duty cycle) of the filter channel. The detection efficiencies have been determined by calibration measurements, as explained in the previous section, and are listed in Table 1, whereas the data acquisition efficiencies ε_{DAQ}^{dc} are simultaneously measured during a run using the scaler values and were on the order of 91 % for pure nitrogen and 96 % for dry air [9].

The only parameters which are finally varied during the global minimization procedure thus are the total number of photons of the main-transitions $N_{dv'}$, the intensity ratios $R_{v',v''}$ and the lifetimes $\tau_{dv'}$ of the initial states v'. If the linear pressure dependence of the reciprocal lifetimes is taken as an additional constraint the lifetime $\tau_{dv'}$ in Eq. (24) is substituted by relation (9) and the intrinsic lifetime $\tau_0^{v'}$ as well as the various quenching rate constants $Q_x^{v'}(T)$ are varied instead. In this way the consistency of the parameters is always ensured.

According to the separation of the excitation and de-excitation processes in Eq. (16) the following data analysis was subdivided into two steps. First, the de-excitation parameters such as intrinsic lifetimes $\tau_0^{v'}$, intensity ratios $R_{v',v''}$ as well as the various quenching rate constants $Q_x^{v'}(T)$ for the different air constituents, were determined using the full usable energy range between 250 keV and 2000 keV to maximize statistics. Afterwards, the obtained values for the de-excitation parameters were fixed and the intrinsic fluorescence yields $Y_{v'}^0(E)$ of the corresponding main-transitions were determined in different energy intervals, to study their energy dependence.

4.2. *Study of De-Excitation Parameters*

The present study concentrates on the eight strongest nitrogen transitions listed in Table 1 which belong to the three independent vibrational sub-systems 2P(0,v''), 2P(1,v'') and 1N(0,v''). To obtain stable and reliable results by the global minimization procedure explained above, at least two nitrogen transitions from different vibrational sub-systems need to be measured separately. With the current filter set this was only possible for the 2P(0,0) transition in channel 4. Nevertheless, the 2P(1,0) transition in channel 1 can also be approximately considered as a pure transition since it contains only small contributions of the 2P(2,1) and 2P(3,2) bands, as can be seen in Fig. 4.

An additional challenge was the measurement of the 1N(0,0) transition in channel 5, since it is contaminated by several weak bands of the higher vibrational transitions 2P(3,6), 2P(2,5) and 2P(1,4). Fortunately, transitions of the 1N system have much longer intrinsic lifetimes and are also more affected by the collisional quenching than the 2P transitions. Therefore the evolution of their time spectra with pressure differs much from the 2P transitions, what helps to separate both band systems from each other. Since only 2P transitions with $v' = 0, 1$ are considered in this analysis, all the other 2P contaminations in channel 5 with $v' > 1$ are merged into the 2P(1,4) transition assuming their pressure dependence to be similar. In this way, the 2P(1,4) transition becomes an effective measure for all 2P transitions in channel 5 and is expected to be more intense than the pure 2P(1,4) transition. In order to avoid negative effects on the results for the 2P transitions in the other filter channels, the analysis was done in two steps. At first, only the 2P-transitions in channels 1 to 4 were simulta-

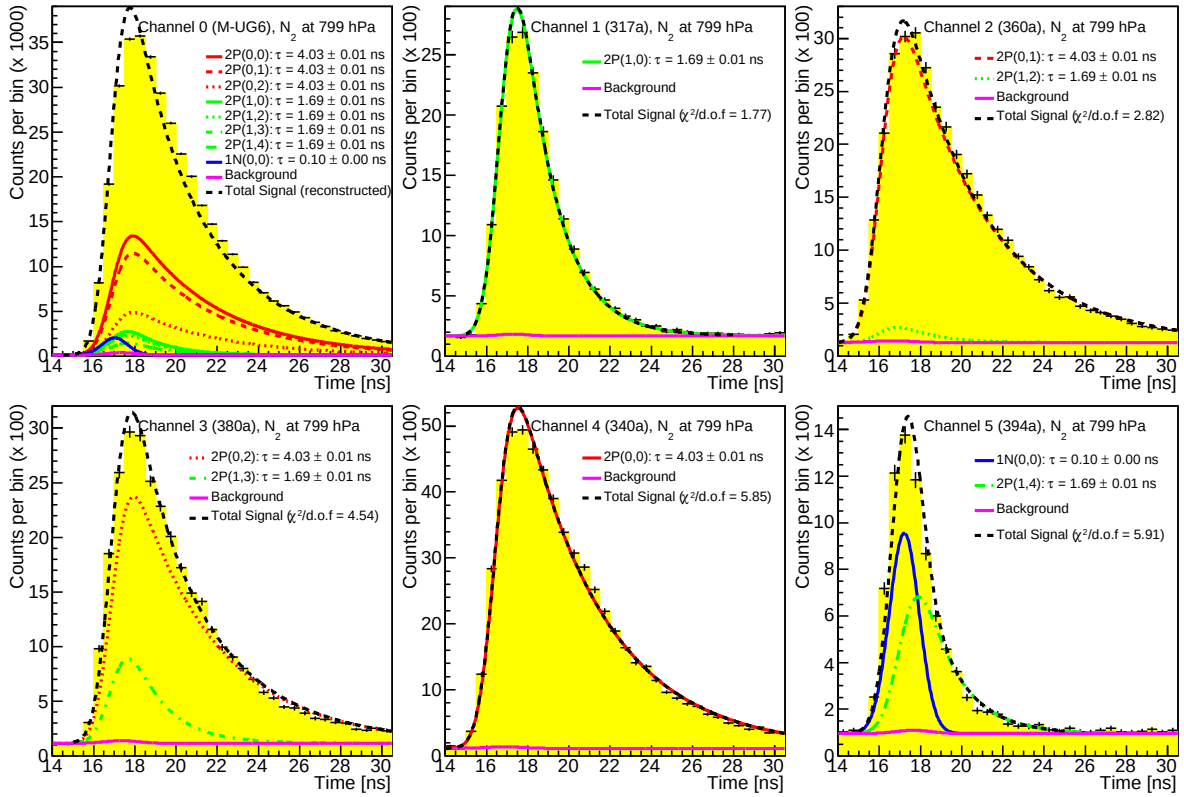

(a) Nitrogen at 800 hPa (smaller time scale!)

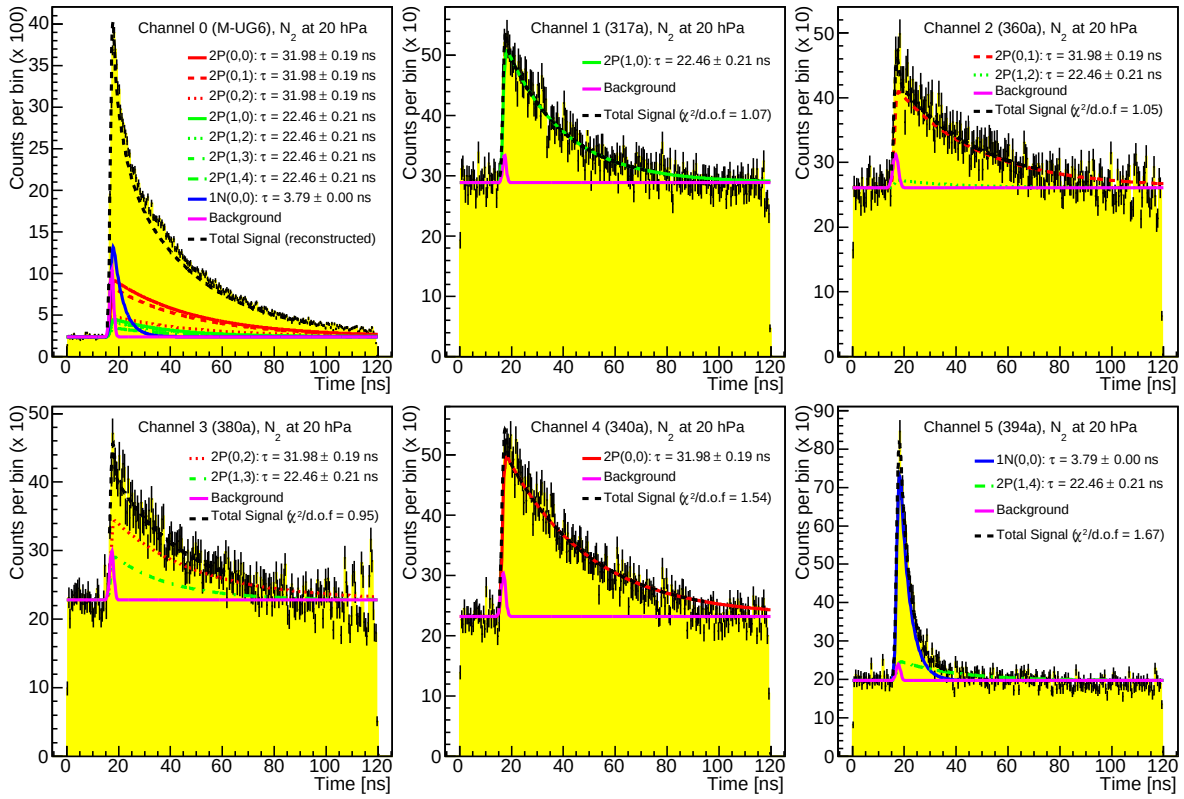

(b) Nitrogen at 20 hPa

Fig. 7. Time spectra in pure nitrogen at 20 hPa and 800 hPa (different time ranges are displayed in both cases). The signal in channel 0 is not fitted but has been reconstructed from the signals in the other channels (see also Fig. 10). For low pressures, the electron correlated background contributions (pink line) are not negligible and have been parametrized by an empirical formula [9].

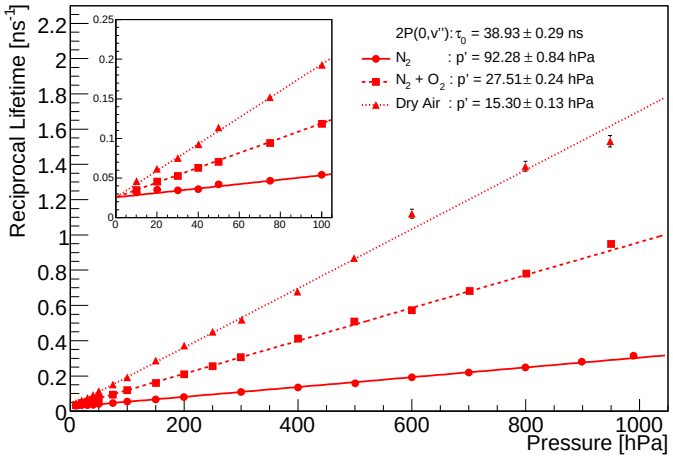

(a) Vibrational level $v' = 0$

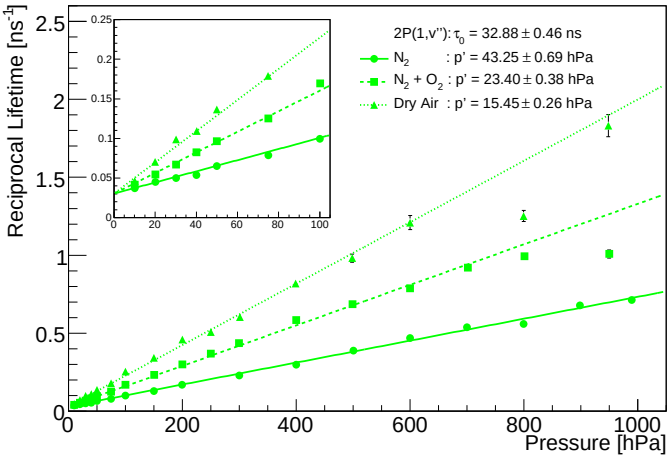

(b) Vibrational level $v' = 1$

Fig. 8. Stern-Vollmer plots of the reciprocal lifetimes for the vibrational states $v' = 0, 1$ of the 2P system. The lines are not a direct fit to the data points but illustrate the pressure dependence derived from the lifetimes and the quenching rate constants, which were obtained by a global minimization with a linear constraint on the reciprocal lifetimes.

neously studied by excluding channel 5 from the analysis. Afterwards, just channel 5 was analyzed, keeping the lifetime of the 2P(1,4) transition in each dataset fixed to the values obtained by the previous analysis of the 2P system.

An example for the resulting contributions in each filter channel is given in Fig. 7 where the time spectra of two datasets in pure nitrogen at pressures of 20 hPa and 800 hPa are shown. Note that for high pressures the time scale is much smaller than for the low pressure measurements. At 20 hPa the 1N(0,0) band in channel 5 is clearly dominating whereas at high pressure the 2P contaminations are of the same order than the 1N(0,0) signal. Channel 0 with the M-UG6 broad band filter is always excluded from the minimization procedure since it may contain other contributions from unknown or disregarded fluorescence transitions. Nevertheless, its signal can be reconstructed with the information from the other channels providing a useful crosscheck of the minimization results as is shown in Section 4.2.3.

4.2.1. *Analysis of the 2P system*

As explained above, only the filter channels 1 to 4 were used to study the quenching parameters of the 2P system. Furthermore, the analysis was restricted to measurements at pressures higher or equal than 10 hPa to avoid systematic effects due to slight gas impurities. The time spectra of 46 runs in nitrogen, artificial air, and the nitrogen-oxygen mixture have been simultaneously fitted by the general minimization function (23). In the first instance the minimization function was only constrained by the universal relations following from the decay law (4). The resulting lifetimes for the vibrational levels $v' = 0, 1$ are reciprocally plotted versus the pressure in the Stern-Vollmer plots shown in Fig. 8. For all gases the data points show a clear linear dependence on the pressure as expected from Eq. (10). Some outliers may be explained by an insufficient separation of different contributions by the minimization procedure. Such effects can be reduced by further constraining the lifetime in Eq. (24) through the linear expression (9), which additionally allows to account for slight temperature variations between different runs. The results of a second minimization, using these constraints, are represented by the lines drawn in Fig. 8. The y-axis intercept is in common for all lines within a graph, indicating the reciprocal intrinsic lifetime of the corresponding initial state v'. The lines are in good agreement with the single data points obtained by the previous minimization without the linear constraint.

This final minimization, with a global reduced χ^2_r of 1.77, leads to a consistent set of intrinsic lifetimes $\tau_0^{v'}$, quenching rate constants $Q_x^{v'}$ and intensity ratios $R_{v',v''}$ which are listed in Tables 2 - 4 together with the results of other authors. The value of 32.9 ns for the intrinsic lifetime of the 2P(1,v'') sub-system seems to be too low compared to the other authors. The reason might be the contamination of the 2P(1,0) main-transition in channel 1 with slight contributions of the 2P(2,1) and 2P(3,2) transitions which cannot be separated by this analysis. This contamination is also supposed to be the main reason for the deviation of the intensity ratios of the 2P(1,v'') sub-system from the theoretical expectations of Gilmore et al. in Table 4.

4.2.2. *Analysis of the 1N system*

The 1N(0,0) transition is the only strong transition of the 1N system between 300 nm and 400 nm which was studied in this work. Due to the reasons explained before, the quenching parameters of this transition were determined by a separate analysis of channel 5 only. To separate the 1N(0,0) transition from the 2P contaminations, the lifetime of the 2P(1,4) transition was fixed in each dataset to the corresponding value taken from the previous analysis of the 2P system, and only the intensity ratio $R_{1,4}$ was allowed to vary during the global minimization procedure.

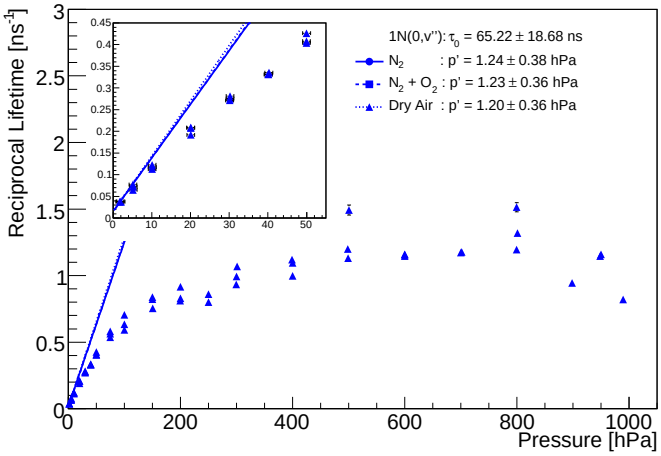

Fig. 9. Stern-Vollmer plot of the reciprocal lifetimes for the 1N(0,v") sub-system. As in Fig. 8 the lines correspond to the pressure dependence obtained by a global minimization with a linear constraint on the reciprocal lifetimes. The deviation between the single data points and the minimization result is due to unseparated 2P-contaminations.

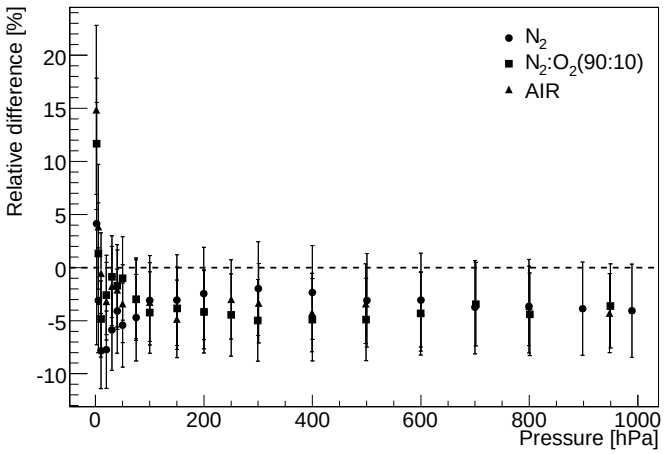

Fig. 10. Relative differences between the reconstructed and the measured signal in channel 0 with the M-UG6 filter (systematic errors are included). From this follows that the contribution of neglected nitrogen bands is less than 4 %.

In contrast to the 2P system, the pressure range could be extended down to 2 hPa since the 1N transitions become much stronger at lower pressures and are also less affected by gas impurities due to the large self-quenching rate of nitrogen. As for the 2P system the minimization was done in two steps with increasing levels of constriction. The first minimization, using only the most general constraints, results in the individual data points for the intrinsic lifetimes shown in the Stern-Vollmer plot in Fig. 9. Compared to the corresponding plots of the 2P system in Fig. 8, a linear behavior is hardly visible. This is caused by an insufficient separation of the 2P contaminations, for pressures larger than 50 hPa. Below this point the data seem to adopt a linear behavior since the intensity of the 1N(0,0) transition becomes strong enough to be silhouetted against the 2P contaminations, as can also be seen in the time distributions of Fig. 7. Therefore only runs between 2 hPa and 50 hPa were considered in the second minimization step in which the lifetimes were additionally constrained by the linear expression (9), as was already done for the 2P system. This minimization resulted in a global reduced χ_r^2 of 1.26 and a set of de-excitation parameters which are listed in Tables 2 - 4 together with the values for the 2P system. It must be stressed again that the intensity ratio of the 2P(1,4) transition in Table 4 is just an effective measure for all 2P contaminations in channel 5. Therefore its value is expected to be larger than for the pure 2P(1,4) transition.

The results of this final minimization are represented by the lines in Fig. 9, which are clearly deviating from the single data points obtained by the first minimization without the linear constraint. Therefore, the separation of the 2P from the 1N contributions in channel 5 only seems to be possible by using all the known physical relations to constrain the minimization function. Furthermore, nearly no difference between the three gas mixtures can be recognized, since the slopes of the lines turn out to be roughly the same. This leads to the conclusion that the quenching of the 1N(0,v'') sub-system is mainly due to nitrogen self-quenching, since the different contributions of oxygen show hardly any effect on the lifetimes.

4.2.3. *Comparison to M-UG6 Data*

The de-excitation parameters determined in the last two sections completely describe the pressure dependence of the relative intensities for the investigated nitrogen transitions. To verify their applicability on the whole atmospheric pressure range, the time spectra of channels 1 to 5 of the complete set of measurements were fitted again with the de-excitation parameters fixed to the values listed in Tables 2 - 4. Only the intensities of the main-transitions were allowed to vary freely in each dataset. Afterwards, the fluorescence signal in channel 0 with the M-UG6 broad band filter was calculated using the fitted intensities and the detection efficiencies (see Table 1) of each transition. An example for the reconstructed time distributions in channel 0 is given by the upper left graphs of Fig. 7 for pure nitrogen at two different pressures. The yellow histograms represent the measured time distributions and the calculated contributions of each nitrogen transition, as well as their sum, are plotted on top of the measured distribution. For both pressures, the signal in channel 0 could be almost completely recovered by the information from the other channels. This worked also for the other gas mixtures and pressures, as is shown in Fig. 10, where the relative differences between the reconstructed and measured integrated fluorescence signals in channel 0 are plotted versus the pressure. The systematic uncertainties are already included in the error bars and the large fluctuations of the data points below 10 hPa can be explained by the limited statistics for low pressure runs. For pressures larger than 10 hPa the data points stabilize and the reconstructed signals are about 4 % smaller, but still compatible with the measured signals. However, a small excess of the measured signal in channel 0 is expected, since

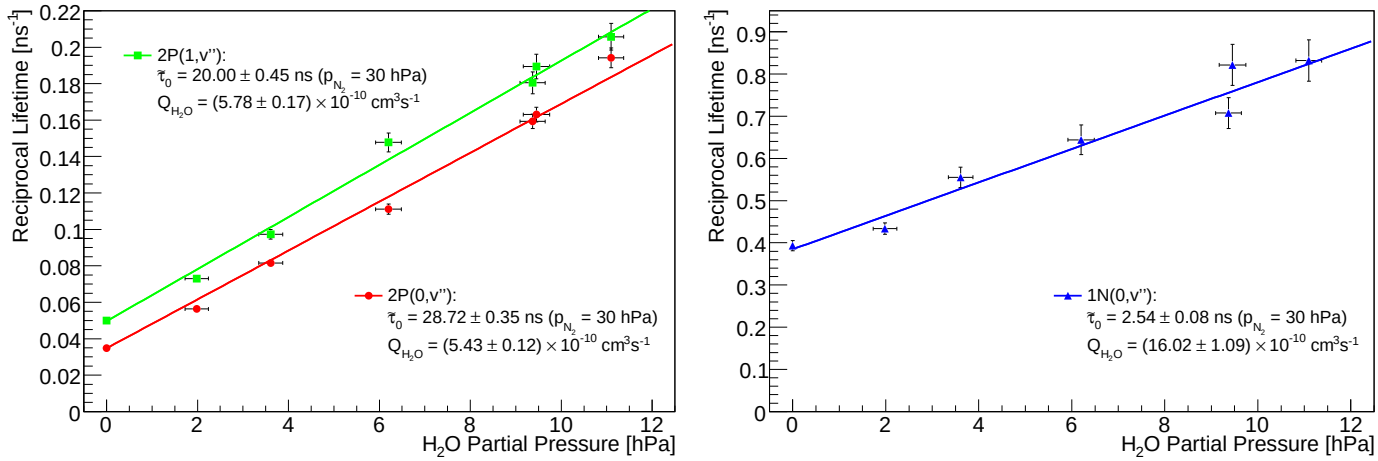

(a) 2P system

(b) 1N system

Fig. 11. Reciprocal lifetimes in humid nitrogen versus the water vapor partial pressure. The nitrogen partial pressure was always kept at 30 hPa. The data points at $p_{\mathrm{H_2O}} = 0$ correspond to the reciprocal lifetimes $1/\tilde{\tau}_0$ in dry nitrogen at a pressure of 30 hPa.

this channel is also measuring transitions which were neglected in the present analysis. From this follows that the contribution of disregarded transitions to the total nitrogen fluorescence spectrum in the M-UG6 filter range is less than 4 %.

4.2.4. *The Effect of Water Vapor*

The influence of water vapor on the nitrogen quenching was studied by adding different concentrations of water vapor to pure nitrogen at a (partial-) pressure of $p_{\mathrm{N_2}} = 30$ hPa. The water vapor concentration was monitored by a calibrated humidity probe [6] which was measuring the relative humidity with an absolute systematic uncertainty of 1.5 % rH. The water vapor partial pressure $p_{\mathrm{H_2O}}$ was derived from the relative humidity according to the magnus formula [9,16]. Six runs were performed at room temperatures between 15 °C and 17 °C and relative humidities ranging from 10 % rH to 60 % rH. Each run lasted for roughly 30 hours but only data of the last ∼ 20 hours was used for the analysis, in order to ensure the water vapor concentration to be in thermal equilibrium with the surrounding chamber walls.

As before, the data analysis was done by simultaneously fitting the time spectra of all datasets with the minimization function (23), by applying only the most general constraints and by fixing the intensity ratios to the values obtained from the previous analysis listed in Table 4. The global reduced χ^2_r of this minimization was 1.09 and the resulting reciprocal lifetimes for the three vibrational subsystems are drawn versus the water vapor partial pressure $p_{\mathrm{H_2O}}$ in Fig. 11. The data points at $p_{\mathrm{H_2O}} = 0$ correspond to the results of the previous analysis for dry nitrogen at a pressure of 30 hPa. According to Eq. (9) the water vapor quenching rate constants $Q^{v'}_{\mathrm{H_2O}}$ were determined through a fit of the linear expression

$$\frac{1}{\tau_{v'}} = \underbrace{\frac{1}{\tau_0^{v'}} + \frac{p_{\mathrm{N_2}}}{kT} \cdot Q^{v'}_{\mathrm{N_2}}}_{=:\,1/\tilde{\tau}_0} + \frac{p_{\mathrm{H_2O}}}{kT} \cdot Q^{v'}_{\mathrm{H_2O}} \tag{25}$$

to the data points in Fig. 11, resulting in the values listed in Table 3. For the 2P system the water vapor quenching rate constants were roughly two times larger than the corresponding values for oxygen, whereas the quenching of the 1N system by water vapor is roughly three times stronger than by nitrogen or oxygen. This large value may be explained by the polar nature of the H_2O and the N_2^+ molecules. Despite of the large values for the water vapor quenching rate constants the effect on the nitrogen quenching in the atmosphere is expected to be rather small since the water vapor concentration in air usually is much lower than the nitrogen or oxygen concentrations.

4.3. *Study of Energy Dependence*

According to Eq. (16) the total number of photons $N_{v',k}$, emitted by a main-transitions $v' \to k$, is related to the intrinsic fluorescence yield $Y^0_{v',k}(E)$ through the expression

$$N_{v',k}(p,T,E) = \frac{\tau_{v'}(p,T)}{\tau_0^{v'}} \cdot Y^0_{v',k}(E) \cdot E_{dep}(E)\ . \tag{26}$$

The lifetime $\tau_{v'}(p,T)$ is only affected by the de-excitation parameters, which are known from the analysis described before. Therefore the last missing quantity for the determination of the intrinsic fluorescence yield is the deposited energy $E_{dep}(E)$ in the chamber volume which was obtained from Monte-Carlo studies described below.

4.3.1. *Energy deposit in Chamber*

A precise knowledge of the energy deposit in the chamber is crucial for the correct determination of the fluorescence yield. In confined volumes, the energy deposit is not

[6] AHLBORN FH A646-E7C

Table 2
Intrinsic lifetimes $\tau_0^{v'}$ in [ns] for the initial states of the investigated vibrational sub-systems. Only statistical errors are quoted.

2P($v'=0$)	2P($v'=1$)	1N($v'=0$)	Reference
38.9 ± 0.3	32.9 ± 0.5	65.2 ± 18.7	this work
42.0 ± 2.0	41.0 ± 3.0	-	Pancheshnyi et al. [17]
41.7 ± 1.4	41.7 ± 2.1	-	Morozov et al. [18]
44.5 ± 6.0	49.3	65.8 ± 3.5	Bunner [3]
37.1*	37.5*	62.3*	Gilmore et al. [14]

* Theoretical values

Table 3
Quenching rate constants $Q_x^{v'}$ in $[10^{-10}\mathrm{cm}^3\mathrm{s}^{-1}]$ for the initial states of the investigated vibrational sub-systems, given for $T = 293K$ ($\sim 20°\mathrm{C}$). Only statistical errors are quoted.

Molecule	2P($v'=0$)	2P($v'=1$)	1N($v'=0$)	Reference
N_2	0.11 ± 0.00	0.29 ± 0.00	5.00 ± 0.17	this work
	0.13 ± 0.02	0.29 ± 0.03	-	Pancheshnyi et al. [17]
	0.12 ± 0.01	0.25 ± 0.01	-	Morozov et al. [18]
	0.10 ± 0.01	0.22 ± 0.03	3.80 ± 0.26	Nagano et al. [5]
	0.07	0.23	2.90	Bunner [3]
O_2	2.76 ± 0.01	2.70 ± 0.03	5.24 ± 0.79	this work
	3.00 ± 0.30	3.10 ± 0.30	-	Pancheshnyi et al. [17]
	2.62 ± 0.19	2.77 ± 0.45	2.39 ± 0.40	Nagano et al. [5]
	1.35	-	8.38	Bunner [3]
H_2O	5.43 ± 0.12	5.78 ± 0.17	16.02 ± 1.09	this work
	3.90 ± 0.40	3.70 ± 0.40	-	Pancheshnyi et al. [17]
	7.10 ± 0.70	6.70 ± 0.70	-	Morozov et al. [18]

Table 4
Intensity ratios $R_{v',v''}$ of the investigated transitions. The values of Bunner have been derived from the fluorescence efficiencies quoted in his work. The second error corresponds to systematic uncertainties of the detection efficiencies.

Transition	this work	Bunner [3]	Fons et al. [19]	Gilmore et al. [14]
2P(0,0)[a]	$1.00 \pm 0.00 \pm 0.00$	1.00	1.00	1.00*
2P(0,1)	$0.69 \pm 0.00 \pm 0.06$	0.75	0.63	0.67*
2P(0,2)	$0.29 \pm 0.00 \pm 0.02$	0.26	0.25	0.27*
2P(1,0)[a]	$1.00 \pm 0.00 \pm 0.00$	1.00	1.00	1.00*
2P(1,2)	$(0.33 \pm 0.03 \pm 0.04)$[b]	0.58	0.45	0.47*
2P(1,3)	$(0.34 \pm 0.01 \pm 0.03)$[b]	0.54	0.43	0.41*
2P(1,4)	$(0.46 \pm 0.02 \pm 0.04)$[c]	0.32	0.16	0.20*

* Theoretical values.

[a] Main-transitions (Ratio equals to one per definition).

[b] Biased value due to contamination of 2P(1,0) band.

[c] Biased value due to contamination of 2P(1,0) and 2P(1,4) bands.

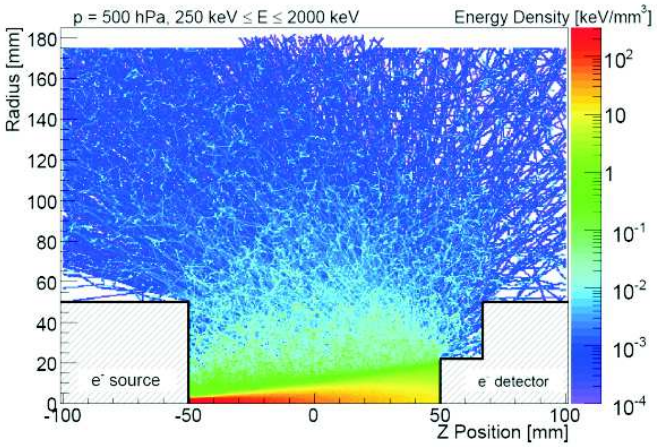

Fig. 12. GEANT4 simulation of the spatial distribution of the deposited energy density within the AirLight chamber at a pressure of 500 hPa, for detected electron energies between 250 keV and 2000 keV.

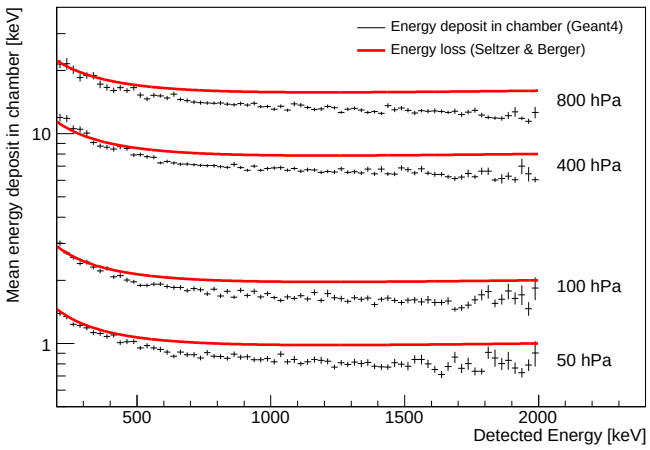

Fig. 13. Mean deposited energy per electron in the chamber versus the detected energy in the scintillator for various pressures. The red lines correspond to the ionization energy loss in dry air given by the Seltzer & Berger formula [21].

necessarily equal to the ionization energy loss, as it follows from the Bethe-Bloch formula, since secondary delta electrons may carry away part of the energy. Furthermore, additional secondary electrons emerging from collisions of the primary electrons with the collimator walls, or electrons repulsing out of the scintillator, may even increase the effective energy deposit. Therefore the energy deposit in the chamber is expected to deviate from the ionization energy loss. Energy losses due to Bremsstrahlung in the gas are negligible at these energies.

To determine the mean energy deposit in the chamber of an electron which was detected with a certain energy in the scintillator, detailed GEANT4 simulations have been performed [9]. The simulations were done using GEANT4 7.1 [20] and the low energy extension for the electromagnetic processes. The simulated ^{90}Sr electron energy spectra were convoluted with the energy resolution function of the scintillation detector and compared to the measured energy spectra. The "facrange" parameter of the multiple scattering model, which affects the penetration depth of the electrons into a new material, had to be tuned to a value of 0.01. This significantly improved the treatment of the electron backscattering within the lead collimator which has to be taken into account in order to produce realistic energy spectra [9]. After the simulation was tested and verified with real electron spectra, several simulations for dry air, at all pressures applied to the real measurements, were performed.

The simulation directly generated two-dimensional histograms of the deposited energy in each volume element of the chamber, with a spatial resolution of 1 mm^3. Each electron, no matter if it is the primary or a secondary electron, contributes to the energy deposition. An example for such an energy deposit map is given in Fig. 12 for detected electron energies ranging from 250 keV to 2000 keV. If the number of emitted fluorescence photons is proportional to the deposited energy, Fig. 12 can be reinterpreted as the spatial distribution of the fluorescence emissions in the chamber. This was done to determine the angular acceptance ε_Ω of the PMTs [9] which was used to calculate the detection efficiencies in Table 1.

In order to study the energy dependence of the energy deposition, several energy deposit maps for successive, 25 keV wide energy intervals were generated. Each map was integrated over the volume of the chamber and divided by the number of detected electrons to derive the mean energy deposit in the chamber per detected electron. In Fig. 13 the mean energy deposit is plotted for several pressures versus the detected electron energy in the scintillator. The comparison to the Seltzer & Berger description [21] for the mean ionization energy loss reveals a 15 % to 20 % decrease for electrons detected with energies larger than 500 keV. Below this point the deposited energy seems to agree with the ionization energy loss suggesting most of the secondary electrons to be stopped within the gas volume of the chamber.

4.3.2. *Intrinsic Yields*

To determine the intrinsic yields $Y^0_{v',k}(E)$ and to study their energy dependence the measured data were divided into seven sub-samples of 250 keV energy intervals covering the range between 250 keV and 2000 keV. Each sub-sample was fitted separately according to the minimization procedure explained in Section 4.1. During the minimization all the de-excitation parameters were fixed to the values listed in Tables 2 - 4 and only the total number of photons $N_{v',k}$ emitted by the main-transitions was allowed to vary freely. Afterwards the intrinsic fluorescence yields $Y^0_{v',k}(E)$ in each energy interval were evaluated by solving Eq. (26) using the total number of photons $N_{v',k}$ from the fit and the deposited energy, which was calculated from the total number of detected electrons multiplied by the mean deposited energy per electron from the simulation studies explained above.

An example for a medium pressure of 400 hPa is given in

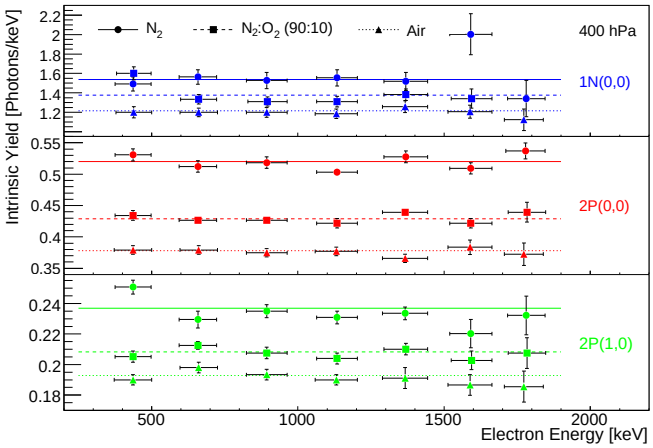

Fig. 14. Energy dependence of the intrinsic fluorescence yields at a pressure of 400 hPa. The horizontal lines are not a direct fit to the data points, but represent the minimization results using the complete energy range.

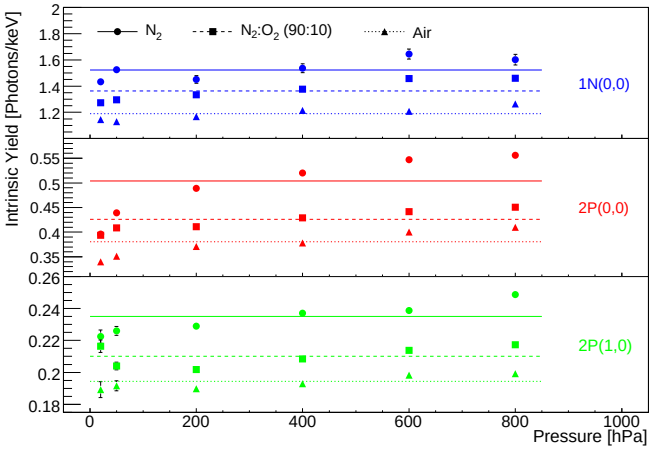

Fig. 15. Pressure dependence of the intrinsic fluorescence yield which presumably is due to experimental deficiencies. The horizontal lines correspond to the values quoted in Table 6 and denote the weighted average of the data points.

Fig. 14 where the intrinsic fluorescence yields of the three main-transitions are plotted versus the electron energies. The relative differences between the intrinsic yields in different nitrogen mixtures seem roughly to scale with the different nitrogen concentrations. Furthermore the intrinsic fluorescence yield appears to be constant over the whole energy range which has been studied. Some fluctuations at high energies can be explained by the reduced statistics due to the β-shape of the electron energy spectrum. In particular between 250 keV and 1000 keV, where the ionization energy loss varies about 30 %, there is no notable change of the intrinsic fluorescence yields. Therefore, the above analysis was repeated using the whole usable energy range between 250 keV and 2000 keV. The results are represented by the horizontal lines in Fig. 14 and agree well with the corresponding data points of the single energy intervals.

To verify the results, this procedure was repeated for several pressures even if a pressure dependence was not expected from the model described in Section 2. It turned out that the intrinsic fluorescence yield apparently decreases for lower pressures as is shown in Fig. 15. The effect is strongest for pure nitrogen and seems to decrease with increasing oxygen concentrations in the other gas mixtures. It could not be clarified if this behavior is a real physical effect or if it is due to experimental issues. Therefore, the final intrinsic fluorescence yield values in Table 6 have been calculated as the weighted average over the data points at different pressures, and are represented by the horizontal lines in Fig. 15. The corresponding systematic uncertainties have been determined as the standard deviation of the single data points to the averaged value and are listed in Table 5. These uncertainties have been quadratically added to the uncertainties of the detection efficiencies in Table 1 to determine the systematic errors quoted in Table 6. Accordingly the final systematic uncertainties for the individual nitrogen bands in air settle between 14 % and 16 %.

Table 5
Systematic uncertainties due to the observed pressure dependence of the intrinsic fluorescence yield.

Gas	2P(0,0)	2P(1,0)	1N(0,0)
N_2	12 %	4 %	5 %
$N_2 : O_2$ (90:10)	5 %	3 %	5 %
Dry Air	7 %	2 %	4 %

5. Results and Discussion

At the beginning of this paper an alternative approach to parametrize the nitrogen fluorescence process in air was introduced. This approach accounts for all physical relations between the different nitrogen emission bands and consistently describes the whole process with a minimal set of parameters. The excitation and de-excitation processes are completely separated by this model and the corresponding parameters have a clear physical meaning. The fluorescence yield in this work is defined in terms of photons per deposited energy. This definition is much closer related to the experimental quantities than the traditional definition in terms of photons per meter track length and additionally allows to account for effects of escaping delta electrons in small volumes. The latter issue especially is important for the absolute determination of the fluorescence yield in small laboratory experiments.

The AirLight experiment synchronously measured the eight strongest nitrogen emission bands between 300 nm and 400 nm for pressures ranging from 2 hPa to 990 hPa with a systematic uncertainty of about 15 %. Furthermore the influence of water vapor on the nitrogen quenching has been studied. The experimental data was analyzed according to the model mentioned before. In the investigated energy range between 250 keV to 2000 keV the fluorescence yield was shown to be independent from the energy of the ionizing electrons.

Table 6
Absolute values of the intrinsic fluorescence yields $Y^0_{v',k}$ in [photons/keV] for the investigated main-transitions $v' \rightarrow k$. The values of this work are valid for electron energies ranging from 250 keV to 2000 keV. The values of Nagano et al. have been converted from his Φ^0-values according to $Y^0 = \frac{\lambda}{\hbar c}\Phi^0$. The second error corresponds to systematic uncertainties.

Gas	2P(0,0)	2P(1,0)	1N(0,0)	Reference
N_2	$0.513 \pm 0.001 \pm 0.096$	$0.236 \pm 0.001 \pm 0.034$	$1.513 \pm 0.014 \pm 0.223$	this work
	$0.318 \pm 0.005 \pm 0.041$	$0.129 \pm 0.007 \pm 0.017$	$0.397 \pm 0.028 \pm 0.052$	Nagano et al. [6]
$N_2 : O_2$ (90 : 10)	$0.429 \pm 0.001 \pm 0.065$	$0.210 \pm 0.001 \pm 0.030$	$1.360 \pm 0.009 \pm 0.200$	this work
	-	-	-	Nagano et al.
Dry air	$0.384 \pm 0.001 \pm 0.061$	$0.195 \pm 0.001 \pm 0.028$	$1.190 \pm 0.008 \pm 0.171$	this work
	$0.272 \pm 0.007 \pm 0.035$	$0.122 \pm 0.007 \pm 0.016$	$0.303 \pm 0.012 \pm 0.039$	Nagano et al. [6]

5.1. *Usage of the Model*

To calculate the fluorescence yield $Y_{v',v''}(p,T)$ for a certain nitrogen transition $v' \rightarrow v''$ at a given temperature T and pressure p the formula

$$Y_{v',v''}(p,T) = Y^0_{v',k} \cdot R_{v',v''} \cdot \frac{\tau_{v'}(p,T)}{\tau_{0\,v'}} \tag{27}$$

applies, where the value of the associated intrinsic fluorescence yield $Y^0_{v',k}$ is listed in Table 6 and the values for the intensity ratio $R_{v',v''}$ and the intrinsic lifetime $\tau_{0v'}$ are tabulated in Table 4 and Table 2 compared to the values of other authors. In this context it should also be referred to the results of the AIRFLY experiment [7] which have recently been published. However, it is strongly advised not to mix the intensity ratios and intrinsic yields from different authors since both quantities are correlated to each other. Even if some intensity ratios of this work, especially for the 2P(1,v'') sub-system, deviate from the values of other authors, they still yield reasonable absolute intensities if they are used together with their associated intrinsic yield values.

The pressure and temperature dependence of the lifetime $\tau_{v'}(p,T)$ in Eq. (27) can be parametrized according to Eq. (9) and result in the following expression for the reciprocal lifetime in air:

$$\frac{1}{\tau_{v'}} = \frac{1}{\tau_{0\,v'}} + \frac{p}{kT} \cdot \Bigg[\Big(0.78 \cdot Q^{v'}_{N_2}(T) + 0.21 \cdot Q^{v'}_{O_2}(T)\Big) \cdot \left(1 - \frac{p_{H_2O}}{p}\right) + \frac{p_{H_2O}}{p} \cdot Q^{v'}_{H_2O}(T) \Bigg] \tag{28}$$

This expression already accounts for the water vapor quenching if the water vapor partial pressure p_{H_2O} is given, which derives from the relative humidity by means of the magnus formula [9,16]. The temperature dependent quenching rate constants $Q^{v'}_x(T)$ can be calculated from the tabulated values in Table 3 by means of Eq. (7).

On the basis of Eq. (27) fluorescence yield spectra can be calculated for the whole pressure and temperature range applying to cosmic ray air shower experiments. An example is given in Fig. 16 where the spectrum for dry air at 4 km height above sea level is compared to the corresponding spectrum of Nagano et al. [6]. The pressure and temperature at 4 km height are computed according to the US Standard Atmosphere [22] and roughly describe the atmospheric conditions as they appear at the shower maximum where most of the energy is deposited in the air.

At a first glance both spectra seem to agree within their errors although there are big differences between the intrinsic yield values in Table 6. This is due to the reason that the de-excitation parameters (intrinsic lifetimes, quenching rate constants) of both experiment are not exactly the same and the intrinsic yield values are calculated in the limit of zero pressure, in order to separate the excitation and de-excitation processes. In pressure ranges where the actual measurements have been performed the agreement between both experiments is much better since the different de-excitation parameters compensate for the differing intrinsic yield values.

The biggest difference in Fig. 16 occurs for the 2P(1,4) transition, which in the present work appears to be too large. This was expected since this work's 2P(1,4) transition is still contaminated by neighboring bands and there-

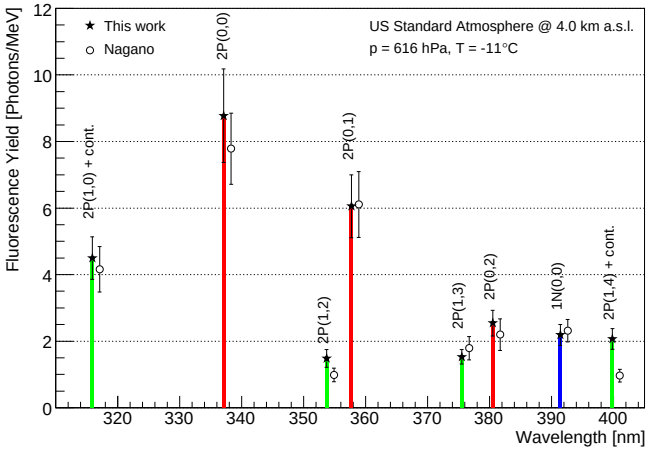

Fig. 16. Absolute fluorescence yield spectrum of the investigated nitrogen transitions in dry air, at atmospheric conditions as they appear at shower maximum, compared to the values of Nagano et al. [6]. The 2P(1,4) and the 2P(1,0) transitions of this work still contain contributions of neighboring bands (see text).

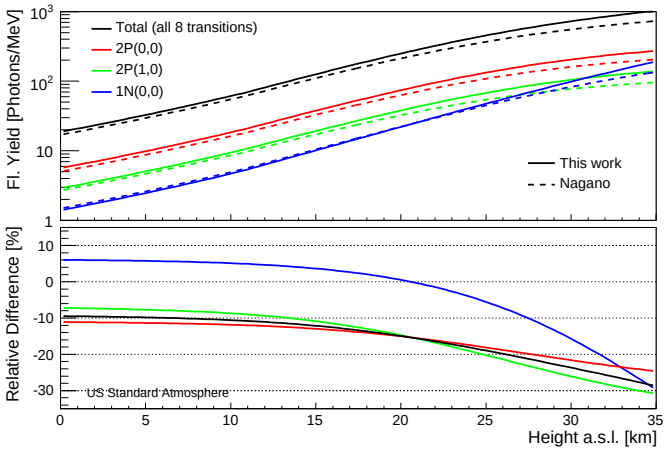

Fig. 17. Fluorescence yield of the three main-transitions and the sum of all investigated transitions versus height a.s.l.. The lower panel shows the relative differences between the values of Nagano et al. and this work in more detail.

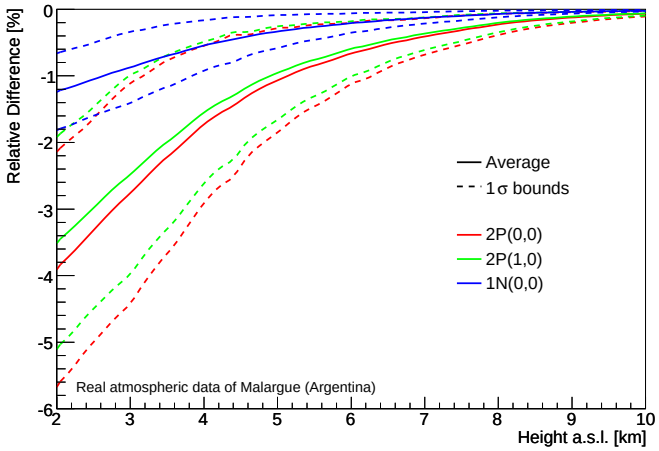

Fig. 18. Relative differences between this work's fluorescence yield with and without taking into account the water vapor content of the atmosphere. Realistic atmospheric profiles from radiosonde launches [23,24] have been used for this comparison.

fore is only an effective measure of all the 2P contributions in the corresponding filter channel. Also the 2P(1,0) transition is known to be slightly contaminated by neighboring bands, however, there seems to be no remarkable difference compared to the spectrum of Nagano et al..

The differences between both spectra become more evident if the fluorescence yield values are compared over a large atmospheric range. In Fig.17 the fluorescence yield of the 2P(0,0), 2P(0,1) and 1N(0,0) main-transitions as well as the sum of all 8 investigated transitions is drawn versus the height above sea level. In the lower regions of the atmosphere this work's fluorescence yield values for the 2P transitions in average are about 10 % larger, whereas the value of the 1N(0,0) transition appears to be 6 % smaller than the corresponding values of Nagano et al.. These deviations are still within the systematic accuracies of both experiments. Above 10 km height the influence of the different de-excitation parameters becomes visible, leading to a slower increase of the values of Nagano et al.. Since the fluorescence light emission in EAS occurs mainly in the lower atmosphere a 10 % difference between both fluorescence models can be expected.

Water vapor in the atmosphere leads to a reduction of the fluorescence yield as shown in Fig. 18, where this work's fluorescence yield is compared for dry and humid atmospheres. Realistic atmospheric profiles, obtained from radiosonde measurements [23,24] at the site of the Pierre Auger Observatory [1] in Malargüe (Argentina), have been used to compute the fluorescence yield with and without taking into account the water vapor concentration. The solid lines correspond to the average of 187 radiosonde launches accomplished in all seasons. The dashed lines indicate the upper and lower bounds of one standard deviation to the average due to the varying water vapor content in the air. At ground level the fluorescence yield of the 2P transitions is 2 % to 5 % lower if the water vapor quenching is taken into account. The 1N transition is only reduced by 1 % to 2 % since its quenching rate in dry air is already relatively large.

These differences are still concealed by the systematic uncertainties of the fluorescence yield but might become an issue if the fluorescence yield is known with a better precision. Currently the main source of uncertainty are the quantum- and collection efficiencies of the PMTs which have only been estimated according to the manufacturers specifications. Therefore, the ongoing work is concentrating on the improvement of the absolute calibration of the experiment using Rayleigh-scattering of a pulsed 337 nm laser, which substitutes the electron beam in the chamber [25]. With this end-to-end calibration of the whole setup, the absolute uncertainties of the fluorescence yield are expected to drop below 10 %.

6. Acknowledgements

The authors are very grateful to Günter Wörner who constructed the chamber and provided excellent expertise in technical matters.

References

[1] J. Abraham, et al., Properties and performance of the prototype instrument for the Pierre Auger Observatory, Nucl. Instr. & Meth. A 523 (2004) 50–95.
[2] R. W. Springer, et al., Recent results from the HiRes air fluorescence experiment, Nucl. Phys. Proc. Suppl. 138 (2005) 307–309.
[3] A. N. Bunner, Cosmic ray detection by atmospheric fluorescence, Ph.D. thesis, Graduate School of Cornell University (February 1967).
[4] F. Kakimoto, et al., A Measurement of the air fluorescence yield, Nucl. Instr. & Meth. A 372 (1996) 527–533.
[5] M. Nagano, K. Kobayakawa, N. Sakaki, K. Ando, Photon yields from nitrogen gas and dry air excited by electrons, Astropart. Phys. 20 (2003) 293–309.
[6] M. Nagano, K. Kobayakawa, N. Sakaki, K. Ando, New measurement on photon yields from air and the application to

the energy estimation of primary cosmic rays, Astropart. Phys. 22 (2004) 235–248.
[7] M. Ave, et al., Measurement of the pressure dependence of air fluorescence emission induced by electrons, Astropart. Phys. 28 (2007) 41–57.
[8] P. Huntemeyer, An experiment to measure the air fluorescence yield in electromagnetic showers, AIP Conf. Proc. 698 (2004) 341–344.
[9] T. Waldenmaier, Spectral resolved measurement of the nitrogen fluorescence yield in air induced by electrons, Ph.D. thesis, University of Karlsruhe (TH) (April 2006).
URL http://bibliothek.fzk.de/zb/berichte/FZKA7209.pdf
[10] A. Ulrich, private communication.
[11] R. W. B. Pearse, A. G. Gaydon, The Identification of Molecular Spectra, Chapman and Hall Ltd, 11 New Fetter Lane, London EC4P 4EE, 1976.
[12] W. A. Bingel, Theorie der Molekülspektren, Verlag Chemie GmbH, Bergsstraße, Weinheim, 1967.
[13] H. Haken, H. C. Wolf, Molekülphysik und Quantenchemie, Springer-Verlag, Berlin Heidelberg New York, 1992.
[14] F. Gilmore, R. R. Laher, P. J. Espy, Franck-Condon factors, r-centroids, electronic transition moments, and Einstein coefficients for many nitrogen and oxygen band systems, J. Phys. Chem. Ref. Data 21 (1992) 1005.
[15] S. Klepser, Optische Elemente des AirLight-Experiments zur spektralen Messung der Fluoreszenzausbeute von Luft, Master's thesis, University of Karlsruhe (TH) (2004).
[16] F. W. Murray, On the Computation of Saturation Vapor Pressure, J. Appl. Meteorol. 6 (1967) 203–204.
[17] S. V. Pancheshnyi, S. M. Starikovskaia, A. Y. Starikovskii, Collisional dectivation of $N_2(C^3\Pi_u, v = 0, 1, 2, 3)$ states by N_2, O_2, H_2 and H_2O molecules, Chem. Physics 262 (2000) 349–357.
[18] A. Morozov, R. Krücken, J. Wieser, A. Ulrich, Gas kinitec studies using a table-top set-up with electron beam excitation: quenching of molecular nitrogen emission by water vapor, Eur. Phys. J. D 33 (2005) 207–211.
[19] T. J. Fons, R. S. Schappe, C. C. Lin, Electron-impact excitation of the second positive band system ($C^3\Pi_u \rightarrow B^3\Pi_g$) and the $C^3\Pi_u$ electronic state of the nitrogen molecule, Phys. Rev. A 53 (4) (1996) 2239–2247.
[20] S. Agostinelli, et al., GEANT4: A simulation toolkit, Nucl. Instr. & Meth. A 506 (2003) 250–303.
[21] S. M. Seltzer, B. M. J., Evaluation of the Collision Stopping Power of Elements and Compounds for Electrons and Positrons, Int. J. Appl. Radiat. Isot. 33 (1982) 1189–1218.
[22] U.S. Standard Atmosphere, U.S. Government Printing Office, Washington, D.C., 1976.
[23] B. Keilhauer, et al., Atmospheric profiles at the southern pierre auger observatory and their relevance to air shower measurement, Proc. 29th Int. Cosmic Ray Conf., Pune 7 (2005) 123.
[24] B. G. Keilhauer, private communication.
[25] D. M. Gonzalez, et al., Laser Calibration of the Air Fluorescence Yield Experiment AIRLIGHT, Proc. 30th Int. Cosmic Ray Conf., Merida.